Military Technical College
Kobry El-Kobba
Cairo, Egypt

12-th International Conference
on
Aerospace Sciences &
Aviation Technology

COMPARISON STUDY OF CLOSURE MODELS FOR MODELING A FLOW ON CURVED AND FLAT PLATES APPLIED TO TURBINE BLADE FILM COOLING.

BERKACHE A[*], **DIZENE R.**[**] and BENMANSOUR S.[**]

ABSTRACT

A numerical study of the interaction of a row of jets of a secondary coolant fluid (R<1) in transverse flow is performed. Discrete jets are arranged across a surface exposed to a wall boundary layer of parallel compressible stream (M_∞=0,72), as occurs in certain discrete-hole cooling systems for turbine blades . The simulation is performed by solving the governing equations numerically, with the effects of turbulence modeled in a way which allows for the anisotropies existing in the real situation and the effects of stream curvature. Comparisons between the results of three turbulence models obtained for injection angle of 45 deg and blowing rate less than unity show discrepancies observed in the flow near the wall. The causes of these differences are identified and discussed.

KEY WORDS

Gas turbine blade, turbulence modeling, compressible crossflow, injection holes, blowing rate, film cooling.

[*] Assistant research, Mechanical Engineering School, USTHB University,
[**] Professor, Mechanical Engineering School, USTHB University,
Advanced Mechanics Laboratory (LMA)
PB. 32, El Alia, 16111, Bab Ezzouar Algiers Algeria, E-Mail: r_dizene@hotmail.com
[**] Professor, Mechanical Engineering School, USTHB University,

NOMENCLATURE

C : Turbulence model constant with various subscripts
D : Jet diameter
G : Production rate of turbulence kinetic energy
k: turbulence kinetic energy
$\bar{p}$: mean static pressure
$\tilde{T}$: mean temperature
$\tilde{T}_e$: crossflow inlet temperature
$\tilde{T}_j$: jet temperature
T^+: non dimensional wall temperature
$\tilde{u},\tilde{v},\tilde{w}$: mean velocity components in Cartesian coordinates
$\tilde{U}_e$: Cossflow inlet velocity
u_i: velocity fluctuation
t : temperature fluctuations
$\tilde{V}_j$: Jet exit velocity
x, y, z : Cartesian coordinates
y_p: distance normal to the wall till the nearest from the wall computational node
y^+: dimensionless value of y, $y^+ = \rho C_\mu^{0.25} k^{0.5} y_p / \mu$
$\overline{u_i u_j}$: Reynolds stresses

Greek symbols
ε : dissipation rate of turbulence kinetic
ω: dissipation frequency rate
μ: Molecular viscosity
μ_t: eddy viscosity
ρ : density
θ : non dimensional temperature
δ: boundary layer thickness
α : jet issuing angle
χ: Von Karman constant
$\sigma_k, \sigma_\varepsilon$: turbulence model constant
τ_w: Wall Shear
~ : Favre (mass-weighted average)
¯ : Reynolds average

INTRODUCTION

Accurate prediction of turbine blade heat transfer, so crucial to the efficient design of blade cooling schemes, still remains important work in the turbomachinery area. The main cause for the lack of agreement with experimental data in such predictions is usually cited to be the turbulence modeling. This is due to a complex flow phenomenon which is encountered in turbine passage and to the interaction of the injection with the aerodynamic curved surface flow around the blades. Stagnation flow heat transfer, heat transfer in the presence of steep pressure gradients both favorable and adverse, free stream turbulence, high Mach number, blowing rate ratio and three-dimensional effects are only some of the items in a long list of phenomena present in these passages.
The experimental flow field and heat transfer measurements are available for the flat plate at many axial locations for fixed inlet Mach number, Reynolds number, inlet turbulence intensity as well as the inlet boundary layer thickness. By far the most popular turbulence models utilized today for flow and heat transfer calculations, are the high and low Reynolds number two-equations eddy viscosity models. The k-ε [1] and k-ω [2] are the most utilized models. These models often offer a good balance between complexity and accuracy.

The ability to predict transition to turbulence which is often present on turbine blades and the ability to integrate to the walls are other reasons for their widely using.
In this paper, numerical simulations have been performed using the Fluent software which is an explicit multigrid finite volume solver, with a k-ε, RSM and SST (shear stress transport) turbulence models. The SST model encompasses both the k-ω model (Wilcox, 1988) activated in the near-wall region and the standard k-ε model (Jones and Launder, 1973) activated in the outer wake region and in the free shear layers. The single row of jets into cross compressible flow interaction is investigated. The jet-to-cross-stream velocity ratio is 0,6 and the Mach number is 0,8. Components of mean and turbulent velocities and the mean temperature are compared with experimental results at upstream and downstream locations in the x–y plane injection. The velocity is nondimensionalized with the cross-stream velocity, while the temperature is represented by the nondimensional local temperature in film.

Cooling turbine blade is an immediate consequence of higher inlet temperature because this is the need for increasing the power output and thermal efficiency of gas turbine engines. Film cooling is commonly employed in order to provide effective blade protection and is realized by injecting coolant jets into the crossflow of hot gases from film cooling holes or slots, on the blade surface. The injected coolant is bent over by the crossflow and forms a film over the blade surface (see Figure 1) and protects the surface from the hot crossflow gases.

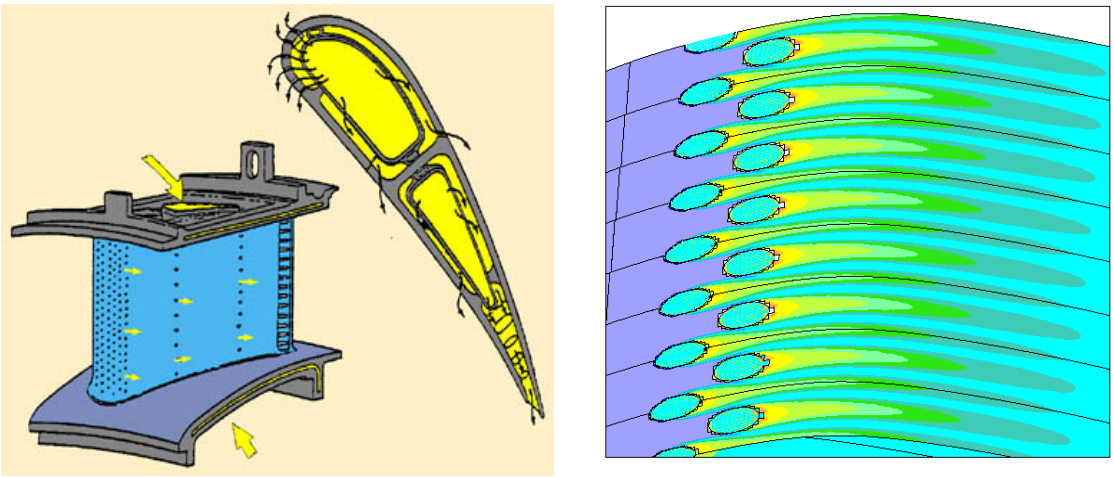

Fig.1. Problem definition and general visualization.

The complex flow field produced by the interaction of the jet and the crossflow has been extensively studied and reported in literature. Experimental studies (Andreopoulos and Rodi, 1984 [3]; Fric and Roshko, 1994 [4] and Dizene et al., 2000 [5,11] ; for example) have revealed that the near field of the jet is highly complex, three dimensional and characterized by large scale coherent structures in the form of jet shear layer vortices which dominate the initial portion of the jet, the horseshoe vortex wrapping around the base of the jet, the counter rotating vortex pair which results from the impulse of the crossflow on the jet and dominate the turbulence structure in formed mixing layer.

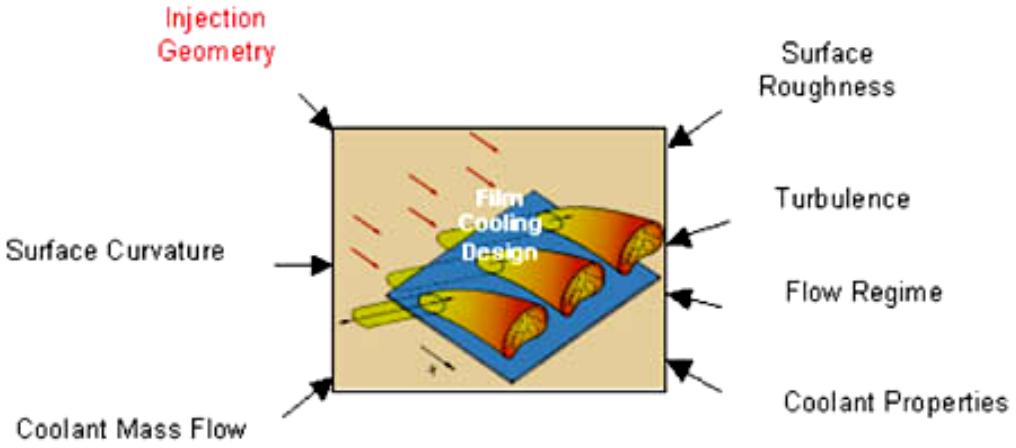

Fig.2. Illustration of a discrete-hole cooling arrangement.

So, strong distortions in jet section results from the counter rotating vortex effects, and the wake vortices formed in the jet wake. The overview of the complex flow field produced by the interaction of the jet and crossflow [5,8] is showed in Figure 3.

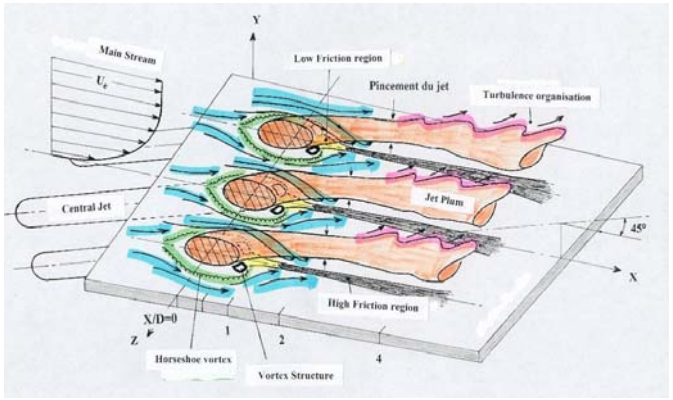

Fig.3. Flow diagram of a row of jets based on experimental results [5,11]

Only a few numerical studies for film cooling flows using second-moment closures have been reported in the literature. Ince and Leschziner [6] carried out an investigation using a high Reynolds RST model employing wall functions in order to avoid solving the Reynolds stresses all the way to the wall. Demuren [7] also reported predictions with a high-Re model using a multigrid method and obtained fairly good prediction of mean flow trends. Jansson and Davidson [9] applied near-wall corrections to the basic linear model and solved a low-Re RST model to predict effusion cooling in a double-row discrete-hole configuration and reported better predictions than a two layer k-ε model.
In the present study we apply four turbulence models to a simple inclined row of jets in a crossflow, compared with the experiments [5,11] in order to evaluate the predictive performances of each of them. The standard linear k-ε model, the RSM and the SST models are applied respectively for flat and convex surfaces. In addition to these models, calculations have been obtained with the non-linear k-ε model and are compared with those of linear model and experiments. The models have therefore been selected with the aim of isolating the influence of these terms and observing the behaviour of the RANS modelling strategy used in this paper.

PROBLEM DESCRIPTION

The film cooling configuration of Dizene et al., [5,11] has been chosen for this study and the corresponding computational domain is shown in Fig.4. In this configuration, inclined simple row of jets is studied. It is expected from Fig.1 that such a flow would be also a good test for turbulence models since, with inclined injection, streamline curvatures are again more pronounced and vorticity generation is enhanced. Simulations have been carried out for a jet Reynolds number of 5.10^5 and a mass flow rate ratio of R = 0,6. These conditions match those of the experimental data of Dizene et al., [5,11]

At the downstream plane, the gradients of all of the dependent variables in the x direction are equal to zero. This fully developed condition was achieved at x/D = 20 [5]. At the symmetric plane (Z = 0) and the holes axis centre (Z = 7.5 mm), the normal gradients of all of the dependent variables are taken to be zero. The flow geometry under consideration and the coordinate system used is shown in Fig. 4. The flow is symmetric about the x – z plane (y = 0).

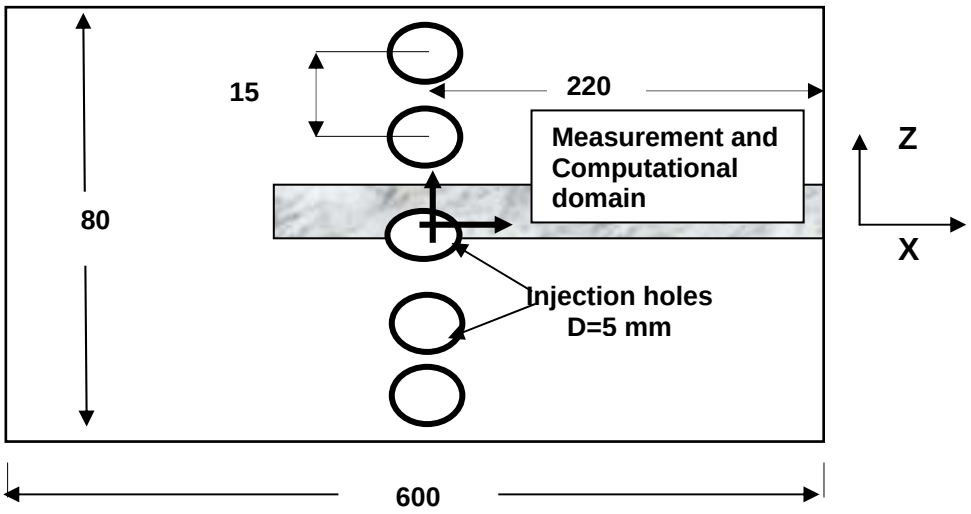

Fig.4a- upper view

Since it has been shown that simplified wall treatments (wall functions, two layer, etc..) or methods that use empirical correlations (low-Re models) cannot correctly capture the shear stresses, the eddy structures and vortices on convex surface. So, we will examine the predictive capability of four turbulence models: standard and non linear k-ε models, RSM and SST models. The governing equations for these various models are listed below.

COMPUTATIONAL ANALISYS

Mathematical formulation

In order to understand the physics of the experimentally flows in interaction, CFD work was carried out. The Navier-Stokes governing the fluid flows in their two-dimensional tensorial form are given below:

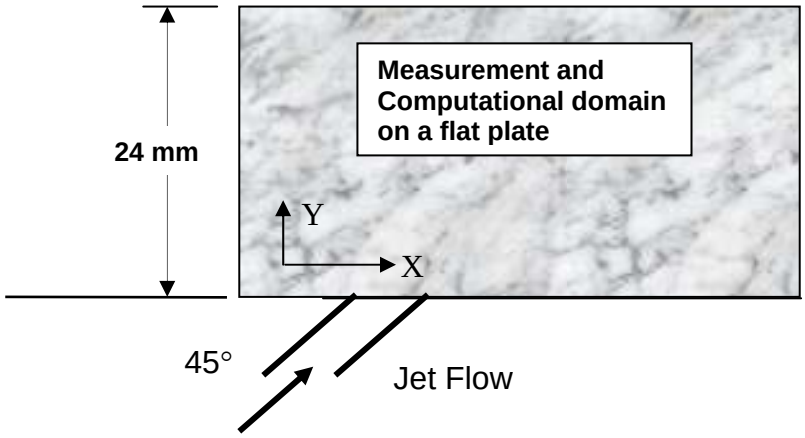

Fig.4b- side view

Fig.4. Schematic diagram of calculation domain and experimental setup [5,11]

$$\frac{\partial \overline{\rho u_i}}{\partial x_j} = 0$$

$$\overline{u}_j \frac{\partial \overline{\rho u_i}}{\partial x_j} = -\frac{\partial \overline{p}}{\partial x_i} + \frac{\partial}{\partial x_j}\left[\rho\nu\left(\frac{\partial \overline{u}_i}{\partial x_j} + \frac{\partial \overline{u}_j}{\partial x_i}\right) - \rho\overline{u_i' u_j'}\right] \qquad (1)$$

To model the turbulence of the flow, four models were used

High-Re k-ε model

In the standard k-ε model (see Launder and Spalding, 1974) the Reynolds stress is modelled as

$$-\rho\overline{u_i' u_j'} = -\frac{2}{3}\rho k \delta_{ij} + 2\mu_t \overline{S_{ij}} \qquad (2)$$

The eddy viscosity μ_t is related to the turbulent kinetic energy k and to its dissipation rate ε as

$$\mu_t = \rho C_\mu \frac{k^2}{\varepsilon} \qquad (3)$$

Equation (2) represents a linear relationship between the turbulent stress and the rate of strain, and forms the basis for all linear two-equation models. Distributions of k and ε in the flow field are determined from their modelled transport equations. The source terms in the modelled equations are given by:

$$S_k = P - \varepsilon \quad ; \quad S_\varepsilon = C_{\varepsilon 1}\frac{\varepsilon}{k}P - C_{\varepsilon 2}\frac{\varepsilon^2}{k} \qquad (4)$$

Where P is the production of turbulence $P = -\rho\overline{u_i' u_j'}\frac{\partial \overline{u}_i}{\partial x_j}$

The standard wall-function approach is thus used to specify the wall boundary

conditions for velocity. For the turbulence kinetic energy a zero value is specified at the wall, while the value of dissipation at a near wall point is set, using a local equilibrium assumption, as $\varepsilon = C_\mu^{3/4} \frac{k^{3/2}}{0.4\delta y}$.

SST model

Menter [16] combines the k-ε and k-ω models in a way that would allow them to be used in the regions where they show to best advantage. In other words, the method uses the k-ω model near the wall, but switches through a function F_1 to the k-ε equations away from the wall, these equations having been transformed to a k-ω format. As indicated by Tulapurkara [17], this method subsequently incorporates Bradshaw's suggestion that the Reynolds shear stress should be taken as being proportional to the turbulent kinetic energy. He calls this model as shear stress transport. The final equations are:

$$\frac{\partial}{\partial t}(\rho k) + \bar{u}_j \frac{\partial}{\partial x_j}(\rho k) = \tau_{ij} \frac{\partial \bar{u}}{\partial x_j} - \beta^* \rho \omega k + \frac{\partial}{\partial x_j}\left[(\mu + \sigma_k \mu_t) \frac{\partial k}{\partial x_j} \right] \tag{5}$$

$$\frac{\partial}{\partial t}(\rho \omega) + \bar{u}_j \frac{\partial}{\partial x_j}(\rho \omega) = \frac{\mu}{\mu_t} \tau_{ij} \frac{\partial \bar{u}}{\partial x_j} - \beta \rho \omega^2 + \frac{\partial}{\partial x_j}\left[(\mu + \sigma_\omega \mu_t) \frac{\partial \omega}{\partial x_j} \right] + 2(1 - F_1) \rho \sigma_{\omega 2} \frac{1}{\omega} \frac{\partial k}{\partial x_i} \frac{\partial \omega}{\partial x_j} \tag{6}$$

The constants in the SST model are calculated as follows. If ϕ is the constant in the SST model and ϕ_1 and ϕ_2 are the constants in the k-ω model and the transformed k-ε model, respectively, then

$$\phi = F_1 \phi_1 + (1 - F_1) \phi_2 \tag{7}$$

The constants in the k-ω are:

σ_{k1} = 0.85, $\sigma_{\omega 1}$ = 0.5, β_1 = 0.075, a_1 = 0.31, β^* = 0.09, K = 0.41, $\gamma_1 = \frac{\beta_1}{\beta^*} - \frac{\sigma_{\omega 1} K^2}{\sqrt{\beta^*}}$

The constants in the transformed k-ε model are:

σ_{k2} = 1.0, $\sigma_{\omega 2}$ = 0.856, β_2 = 0.0828, β^* = 0.09, K = 0.41, $\gamma_1 = \frac{\beta_2}{\beta^*} - \frac{\sigma_{\omega 2} K^2}{\sqrt{\beta^*}}$

τ_{ij} is given by Equation: $-\rho \overline{u_i' u_j'} = -\frac{2}{3} \rho k \delta_{ij} + \mu_t \left(\frac{\partial \bar{u}_i}{\partial x_j} + \frac{\partial \bar{u}_j}{\partial x_i} \right)$; $F_1 = \tanh(\arg_1^4)$:

$$\arg_1 = \min\left[\max\left(\frac{\sqrt{k}}{0.09 \omega y}, \frac{500 \nu}{y^2 \omega} \right), \frac{4 \rho \sigma_{\omega 2} k}{C D_{k\omega} y^2} \right]$$

$$CD_{k\omega} = \max\left(2\rho\sigma_{\omega 2}\frac{1}{\omega}\frac{\partial k}{\partial x_j}\frac{\partial \omega}{\partial x_i}, 10^{-10}\right), \nu_t = \frac{a_1 k}{\max(a_1\omega, \Omega F_1)}$$

$F_2 = \tanh(\arg_2^2)$, $\arg_2 = \max\left(2\frac{\sqrt{k}}{0.09\omega y}, \frac{500\nu}{y^2\omega}\right)$.

Reynolds stress model

The two equation models have been successful in correctly predicting velocity distributions in many situations and are incorporated in commercial codes. However, they need corrections when the flow is subjected to severe adverse pressure gradient and streamline curvature. To overcome these deficiencies, models of turbulence which express the higher-order correlation in the equation for Reynolds stresses were formulated. These Reynolds stresses are given in tensor notation as:

$$u_k \frac{\partial \overline{u_i' u_j'}}{\partial x_k} = P_{ij} + D_{ij}{}^{\mu} + D_{ij}{}^{T} + \phi_{ij} - \varepsilon_{ij} \quad (8)$$

The production, P_{ij} and viscous diffusion D^{μ}_{ij} are treated exactly whereas the turbulent diffusion, D^{T}_{ij}; the pressure-strain correlation, ϕ_{ij} and the dissipation rate ε_{ij} require a modelling approximation for their closure. Most low-Re formulations adopt the following classical decomposition for the pressure-strain correlation:

$$\phi_{ij} = \phi_{ij,1} + \phi_{ij,2} + \phi_{ij,w} \quad (9)$$

Where, $\phi_{ij,1}$ is termed as the slow part involving fluctuating quantities, $\phi_{ij,2}$ is the fast part involving mean strain and $\phi_{ij,w}$ is the wall correction term representing the pressure reflection effects. A consistent form of the dissipation correlation satisfying wall limiting behaviour is written as:

$$\varepsilon_{ij} = (1 - f_s)\frac{2}{3}\varepsilon\delta_{ij} + f_s\varepsilon\frac{\overline{u_i u_j}}{k} \quad (10)$$

Computational domain and boundary conditions

The modelled transport equations were solved using a two-dimensional CFD FLUENT6.0 code based on the SIMPLER algorithm. A non-uniform staggered grid and 33060 mesh cells including the jet injection region are set up in computational domain shown in Fig.5. The topology of the C-type grid used in this study is described by the rectangular west external boundary is corresponding to the inlet and outlet regions, the east boundary is corresponding to the NACA surface and the south and north internal grid lines forming the connection region to close the C-topology. The inlet region (part of west boundary) and the exit region (also part of west boundary) were placed respectively far upstream and downstream of the leading and trailing edge of the profile.

One major step in simulating fluid flows with turbulence model is the choice of appropriate inlet values of the solved primary variables u, v, k, ε or ω for the flow entering the computational domain. The boundary conditions are derived from the experimental measurements. On the jet exit surface, the u and the v velocities are defined, while the w velocity assumes zero value. In the upstream boundary, the u velocity profile, k and ε profiles are also specified in the case of the boundary layer

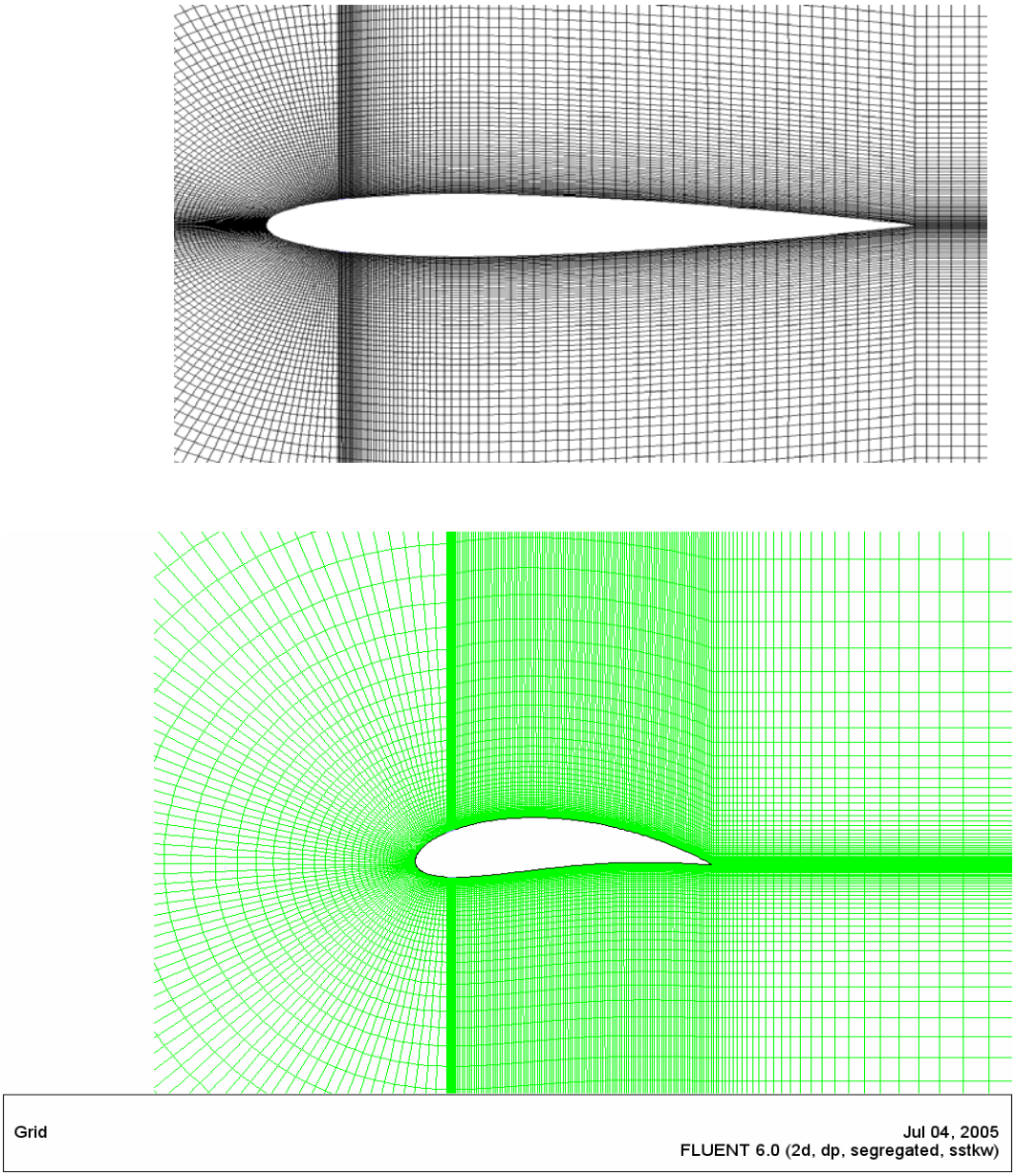

Fig.5 . Views of the computational domain used in the present work

flow. The u velocity is taken in the external flow, while k and ε are calculated. Finally, the temperatures are defined in the jet and the wind tunnel inlet. The upstream and downstream conditions have zero gradients for all states variables. A summary of the boundary conditions is listed in table 1.

Table 1. boundary conditions

Flow Param.	Wall	Upstream	Hole	Downstream	Freestream
$\tilde{U}$	0	$\tilde{U} = \tilde{U}_e(y/\delta)^{1/7}$ if $y \le \delta$ $\tilde{U} = \tilde{U}_e$, $\tilde{U}_e = 248$	$\tilde{U} = \tilde{V}_j \cos(\alpha)$ $\alpha = 45^\circ$	$\partial\tilde{U}/\partial x = 0$	$\partial\tilde{U}/\partial z = 0$ $\partial\tilde{U}/\partial y = 0$
$\tilde{V}$	0	$\tilde{V} = 0$	$\tilde{V} = \tilde{v}_j \sin(\alpha)$ $\tilde{V}_j = \rho_e \tilde{U}_e R/\rho_j$	$\partial\tilde{V}/\partial x = 0$	$\partial\tilde{V}/\partial z = 0$ $\partial\tilde{V}/\partial y = 0$
$\tilde{W}$	0	$\tilde{W} = 0$	0	$\partial\tilde{W}/\partial x = 0$	$\partial\tilde{W}/\partial z = 0$ $\partial\tilde{W}/\partial y = 0$
$\tilde{T}$	$\tilde{T} = \tilde{T}_p$ $\tilde{T}_p = 313^\circ K$	$\tilde{T} = \tilde{T}_p + (\tilde{T}_e - \tilde{T}_p)(y/\delta_T)^{(1/5)}$ $\tilde{T} = \tilde{T}_e$, $\tilde{T}_e = 262^\circ K$	$\tilde{T} = \tilde{T}_j$, $\tilde{T}_j = 327^\circ K$	$\partial\tilde{T}/\partial x = 0$	$\partial\tilde{T}/\partial z = 0$ $\partial\tilde{T}/\partial y = 0$
K	0	$k = C_\mu^{-0.5} l_m \left(\partial\tilde{U}/\partial y\right)^2$, $l_m = \min(\chi y_p, 0.09\delta)$ $k = 1.5 * \tilde{u}^2$	$k = 0.005\tilde{U}_e$	$\partial k/\partial x = 0$	$\partial k/\partial z = 0$ $\partial k/\partial y = 0$
$\tilde{\varepsilon}$	0	$\tilde{\varepsilon} = k^{1.5}/(C_\mu^{-0.75} l_m)$ $\tilde{\varepsilon} = (C_\mu^{0.75} k^{1.5})/(0.09\delta)$	$\tilde{\varepsilon} = k^{1.5}/(0.3 * 0.5 * D)$	$\partial\varepsilon/\partial x = 0$	$\partial\varepsilon/\partial z = 0$ $\partial\varepsilon/\partial y = 0$

RESULTS AND DISCUSSIONS

Results from RANS calculations will be presented first to determine the ability of the various turbulence models to capture the flow physics accurately, and to highlight the effect of curvature on the predicted flow.

Figure 6 shows the surface curvature effects on the mean axial velocity along the jet centreplane (Z/D) = 0) at X=2D; 4D; 6D and 20D axial locations obtained by the SST model for NACA0012 (symmetrical profile with 12% of relative thickness; NACA6512 (relative thickness 12% and 50% of maximum camber); NACA8520 (20% of relative thickness and 50% of maximum camber) airfoils. The profiles are in general similar but not similar to the effect of curvature. The NACA0012 and NACA6512 profiles present high over velocity upper the wall than the NACA8520

The streamwise velocity is over-predicted by the all models. The best prediction here is shown by the RSM and SST models on the wall region at all the locations. But outer of the wall and from Y/d = 0.5 the best prediction is shown by the k-ε.

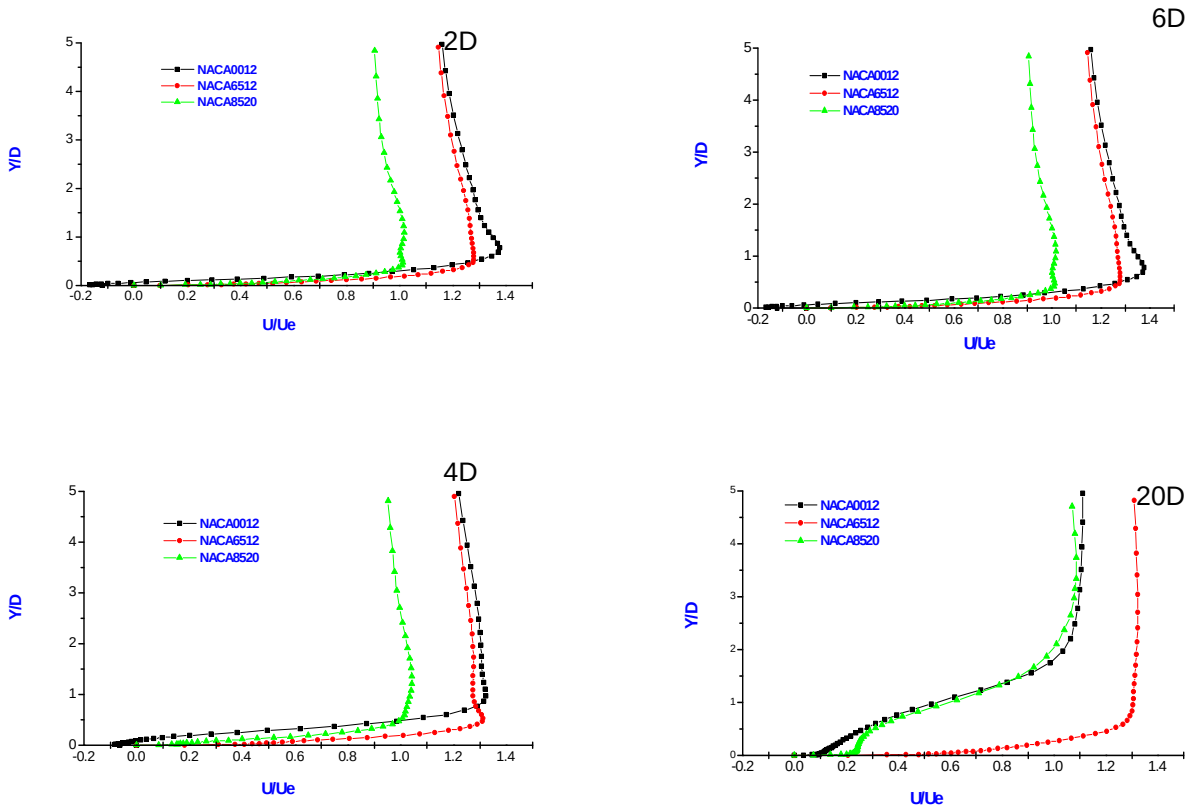

Fig.6. Comparison between predicted longitudinal component profiles of mean velocity in x – y plane. SST model for NACA0012 ; NACA6512 ; NACA8520

Figure 7 shows the turbulence kinetic energy along the jet centreplane (Z/D) = 0) at. X=2D; 4D; 6D and 20D axial locations obtained by the SST model for NACA0012 ; NACA6512 ; NACA8520 airfoils. In the near field of the jet, and in the wake region, where the large scales play an important role in the mixing process, the turbulence kinetic energy is very high on the NACA0012 profile than on the two others.
over-predicted by the k-ε and the RSM models in comparison with the SST model. The best prediction is shown by the SST model in the region between X/D = 1 and X/D = 6.

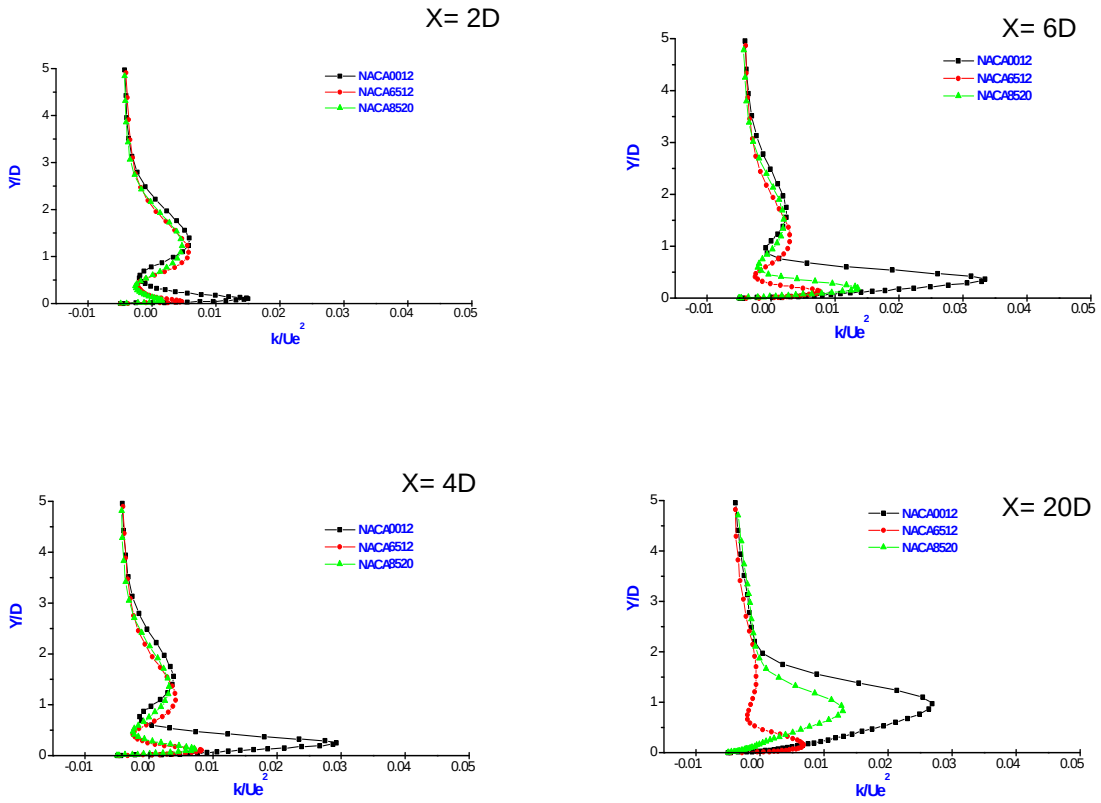

Fig.7. Comparison between predicted kinetic turbulence energy profiles in x – y plane. SST model for NACA0012 ; NACA6512 ; NACA8520

The SST model has been shown to give results for flows with strong adverse pressure gradients that are far superior to those obtained with either the standard k-ε or k-ω models.

Figure 8 shows the turbulence kinetic energy along the jet centreplane (Z/D) = 0) at several axial locations in comparison between the three models predictions. In the near field of the jet, and in the wake region, where the large scales play an important role in the mixing process, the turbulence kinetic energy is over-predicted by the k-ε and the RSM models in comparison with the SST model. The best prediction is shown by the SST model in the region between X/D = 1 and X/D = 6.

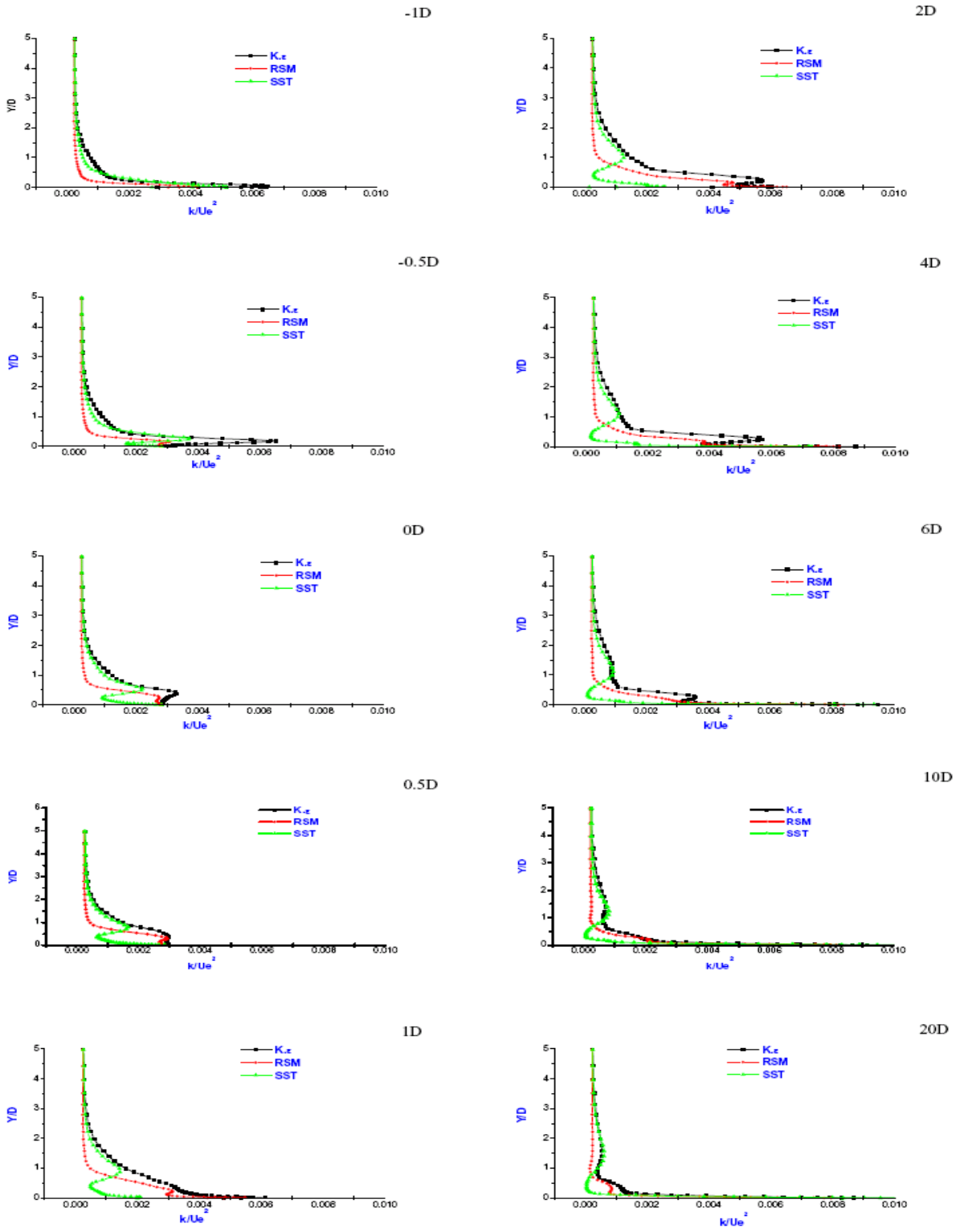

Fig.8. Turbulent field distribution. Kinetic energy profiles. Numerical calculations between linear k-ε, SST and RSM models.

CONCLUSION

In this paper we have presented RANS simulations to estimate the capability of some turbulence models to capture the interaction behaviour of discrete jets with transverse flow under the curvature effect. This study has not incorporated into the simulations the film holes and their duct. The only averaged flow variables are captured and discussed. The effect of curvature is found different in a low cambered airfoil. Higher irregularity pattern of velocity profiles close to the wall may be attributed to the curvature effect and the capability of each model.
The over-prediction of the mean axial velocity may be explained by the ability of RSM and SST models to capture the energy production and transport associated with the coherent scales but over than shown by the experiments, we can not explain this. The RSM predictions do not show any significant improvement over the SST model. This can points to the fact that the anisotropy in the flow turbulence and the effects of the streamlines curvature are not the major contributor to the lack of agreement and the discrepancy may comes from the inability of the RANS method to make a difference between large and low scales or the large scale unsteadiness.

REFERENCES

1 B.E. Launder, D.B. Spalding ‘The numerical computation of Turbulent Flows’. Comp. Math. In Applied Mechanical Engineering, Vol. 3 pp. 269-289, 1974.
2 D.C. Wilcox. “Multiscale model for turbulent flows”. In AIAA 24th Aerospace Sciences Meeting. American Institute of Aeronautics and Astronautics, 1986.
3 J. Andreopolous, W. Rodi ‘Experimental investigation of jets in a cross-flow’. J. Fluid Mech. 138, 93-127, 1984.
4 T.F. Fric, A. Roshko, ‘Structure in the near Field of the Transverse Jet’. Tenth symposium on turbulent shear flows, Oxford University., 1989.
5 R. Dizene. ‘Etude Expérimentale d’interaction de Jets avec un Ecoulement Transversal Compressible. Deuxième partie : Rangée de Jets Obliques’. *Thèse*, CEAT, Université de Poitiers France, 1993.
6 N.Z.. Ince and M.A. Leschziner : "Comparison of Three-dimensional Jets in crossflow with and without Impingement using Reynolds Stress Transport Closure " AGARD symposium on computational and experimental assessment of Jets in Crossflow, 1993.
7 A.O. Demuren: "Modelling jets in cross flow" NASA Contractor Report 194965, ICASE Report N°94-71, Contract NAS1-19480, August 1994.
8 L. S. Jansson & L. Davidson: "Numerical study of effusion cooling in a double-row discrete-hole configuration using a low-Re Reynolds stress transport model" in “Engineering turbulence modelling and experiments III”, eds W. RODI and G. BERGELES, Elsevier Science B.V., 1996.
9 J.M. Charbonnier. ‘Etude Expérimentale et Numérique d’une Interaction d’un Jet droit avec un Ecoulement Transversal Subsonique’. *Thèse*, CEAT, Université de Poitiers, 1992.
10 J.L. Bousgarbies, E. Foucault, J.J. Vuillerme, E. Dorignac. ‘Etude de l’Interaction Jets/Ecoulement en Paroi Plane. Refroidissement des aubes de Turbines par Jets’. *Rapport Contrat DRET 89273,* CEAT-LEA, Poitiers, 1991.
11 R. Dizene, E. Dorignac, J.M. Charbonnier, R. Leblanc. ‘Etude Expérimentale d’interaction de Jets avec un Ecoulement Transversal Compressible. II. Effet

du Taux d'injection sur les Transferts Thermiques en Surface'. *Int. Journal of Thermal Science*, Vol.39 N°5: 571-581, 2000.

12 G.D. Catalano, K.S. Chang, J.A. Mathis. 'Investigation of Turbulent Jet Impingement in a Confined Crossflow'. *AIAA Journal*, Vol. 27 N°11:1530-1535, 1989.

13 K.R. Roth. 'Evaluation of a Navier-Stokes Prediction of a Jet in a Crossflow'. *Journal of Aircraft*, Vol.29,N°2: 185-193, 1992.

14 A. Berkache, 'Comparative study some of closure models for modeling a flow field in interaction with discrete jets'. Master thesis, USTHB university, mechanical engineering school, 2005.

15 R. DIZENE, O. Berkache; D. Cherrared; E.G. Filali and S. Benmansour. 'Numerical Calculation of a row of Jets in Crossflow using k-ε, SST and RSM models. Comparison with the Experiments'. Energy: production, distribution and conservation. Proceedings of the ASME-ATI, Milan may 14/17th, 2006. Biblioteca Termotecnica N°34.

16 F.R. Menter 'Two-equation Eddy-viscosity Turbulence Models for Engineering Applications', AIAA Journal, Vol. 32, pp. 1598-1605,1994.

17 E.G. Tulapurkara, 'Turbulence Models For the Computation of Flow past Airplanes', Prog. Aerospace Sci. Vol. 33, pp. 71-165, 1997.